

Coordinated Control of Offshore Wind Farm and Onshore HVDC Converter for Effective Power Oscillation Damping

Yousef Pipelzadeh, *Member, IEEE*, Nilanjan Ray Chaudhuri, *Senior Member, IEEE*, Balarko Chaudhuri, *Senior Member, IEEE*, and Tim C. Green, *Senior Member, IEEE*

Abstract—Damping contribution from wind farms (WFs) is likely to become a mandatory requirement as a part of the grid codes. For remote offshore WF, connected through a voltage source converter (VSC)-based direct current link, the most convenient option for the onshore transmission system operator (TSO) is to modulate the reactive power at the onshore VSC within their own jurisdiction. In this paper, we show that supplementary control through the onshore VSC alone, although attractive for TSOs, could result in undesirable voltage variations in the onshore grid. On the other hand, modulation of active power output of the wind turbine generators (WTG) alone turns out to be inadequate due to the limited overload capability of the WTGs. Coordinated control over both onshore VSC and aggregated WF output overcomes the above limitations and is shown to be effective for power oscillation damping. A homotopy approach is used to design the coordinated controller, which can be implemented locally (at offshore WF and onshore converter site) using a decentralized architecture. This is a bilinear matrix inequality problem, which is solved by transforming these constraints into linear matrix inequality constraints. Case studies on two test systems show that the proposed controller yields similar system dynamic response as supplementary control through the WF alone.

Index Terms—Bilinear matrix inequality, decentralized control, homotopy, HVDC, linear matrix inequality, offshore wind, power oscillation damping, residues, voltage source converter.

I. INTRODUCTION

THE ability from offshore wind farms connected via Voltage Source Converter-based High Voltage Direct Current (VSC-HVDC) to provide ancillary services is an important consideration for systems with high wind penetration. With increasing number of offshore wind turbine installations worldwide, transmission system operators (TSO) have established revised grid code requirements for wind farms

connection. These grid codes [1] require wind farms to provide ancillary services such as inertial support and frequency regulation which are usually demanded from synchronous generators. The European Network of Transmission System Operators (ENTSO-E) has developed the network code for HVDC connections and DC-connected Power Park Modules (PPMs) that include the provision of power oscillation damping (POD) through HVDC, PPMs and coordination thereof [1]. Need of such grid codes in future is also outlined in [2].

Power oscillation damping through WF-based PSS has been reported in literature [3]–[10], mostly in the context of onshore wind turbines connected directly to the AC grid. Much less attention has been focused on power oscillation damping contribution from offshore WF connected to the onshore grid through a VSC-HVDC link. In [11], factors affecting the damping capability of a VSC-HVDC connected offshore WF were carefully considered from a practical standpoint. Potential interactions with AVRs in the system were investigated in depth. A classical phase compensation approach was used to derive the parameters of the POD, which is insightful for a simple system with one poorly damped mode. However, it is not straightforward to extend this approach for more complex systems with multiple poorly damped inter-area modes. Also, coordination between active and reactive power modulation has not been considered in [11]. In this paper, a systematic way of designing a coordinated POD (henceforth referred to as Coordinated PSS) is demonstrated to improve the damping of multiple inter-area modes (Case study II in Section VI).

For remote offshore WFs, connected through a VSC-based DC-link to a transmission system, the preferred option for the onshore TSO is to modulate the reactive power at the onshore VSC station. This avoids the need for supplementary control of offshore WF and thus, dependence on the offshore transmission owner (OFTO). However, this could result in unacceptable voltage variations in the onshore power grid, which will be demonstrated in this paper. On the other hand, modulation of active power output of the wind turbine generators (WTG) alone turns out to be inadequate due to the limited short-term (some percent for few seconds) dynamic overload capability of particular WTGs when operating in the partial or full-load range [12].

To get around the aforementioned problems, coordinated control of the real power reference of the offshore WF and the reactive power reference of the onshore VSC-HVDC converter

Manuscript received December 4, 2015; revised April 8, 2016; accepted June 12, 2016. Date of publication September 27, 2016; date of current version April 17, 2017. This work was supported in part by the Engineering and Physical Sciences Research Council, U.K. under Grant EP/M015025/1 and Grant EP/K006312/1. Paper no. TPWRS-01736-2015.

Y. Pipelzadeh, B. Chaudhuri, and T. C. Green are with the Control and Power Research Group, Imperial College London, London SW7 2AZ, U.K. (e-mail: y.pipelzadeh08@imperial.ac.uk; b.chaudhuri@imperial.ac.uk; t.green@imperial.ac.uk).

N. R. Chaudhuri is with the Department of Electrical Engineering & Computer Science, Pennsylvania State University, State College, PA 16801 USA (e-mail: NUC88@psu.edu).

Color versions of one or more of the figures in this paper are available online at <http://ieeexplore.ieee.org>.

Digital Object Identifier 10.1109/TPWRS.2016.2581984

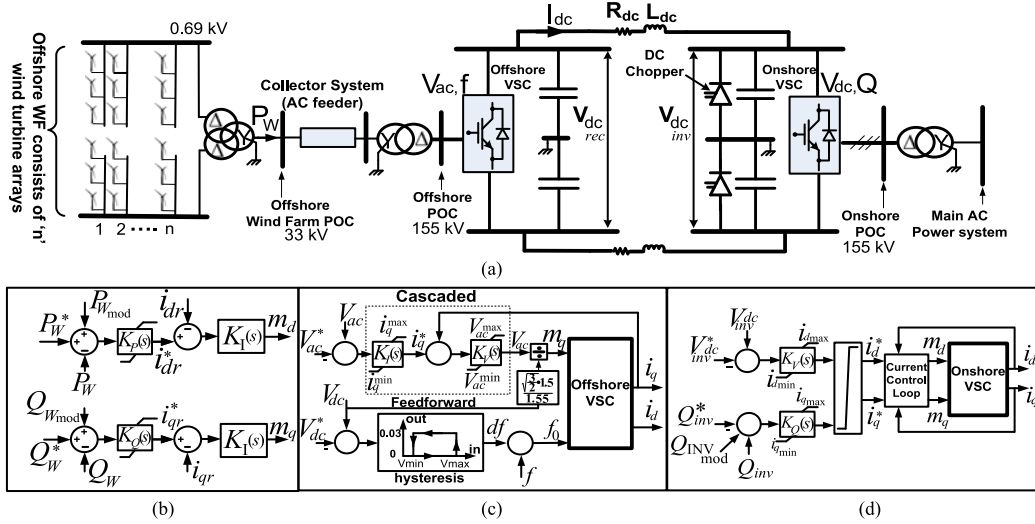


Fig. 1. (a) Schematic of an offshore WF connected to a mainland AC grid through VSC-HVDC link, (b) WF Rotor Side Converter (RSC) control, (c) Offshore converter $V_{ac} - f$ control, (d) Onshore converter $V_{dc} - Q$ control. Control options for supplementary PSS through WF and HVDC are shown.

is proposed. One approach to achieve coordinated control is to design the control-loops simultaneously in a multi-variable framework [13], [14]. However, the resulting full-structure controller is difficult to implement in a decentralized architecture as it requires all the feedback signals, some or all of which could be from remote locations, to be transmitted to each actuator location. On the other hand, if the control structure is block-diagonal, the individual control loops are decoupled from each other, which is easier to implement in a decentralized architecture. Here the concept of homotopy [15] is applied and an extension proposed to obtain a single block-diagonal controller from a full-structure controller designed to ensure specified closed-loop performance.

The main contributions of this paper are the following:

- 1) Coordinated control of offshore wind farm and onshore VSC for effective power oscillation damping is proposed and demonstrated for the first time.
- 2) Homotopy approach is applied for coordinated control design with a decentralized control structure.
- 3) Homotopy design formulation is extended to consider multiple operating conditions for design robustness.

The organization of the paper is as follows: First, the modelling and control of the VSC-HVDC-connected offshore wind farm is presented followed by different choices of PSSs and their operational constraints. Next, the design of robust block-diagonal coordinated PSSs using Homotopy approach is described. Finally two case studies are presented on a 4-machine, 2-area and a 14-machine, 5-area system, respectively. The simulation results demonstrate the effectiveness of the proposed coordinated approach.

II. MODELLING AND CONTROL OF VSC-HVDC-CONNECTED OFFSHORE WIND FARM

An offshore wind farm (WF) connected to an AC grid via VSC-HVDC link is shown in Fig. 1(a). The VSC-HVDC system and the converters were represented by their averaged model which can equally well represent the low frequency characteristics of multi-level or 2-level PWM waveforms even though the

switching frequency difference is marked. The further difference in filter provision and internal energy balancing control were not considered and are scheme specific. The WF model is a generic Type-3 WTG model which includes the aerodynamic, pitch and power plant control model [16]. Description of the modelling and control implementations in DIGSILENT Power Factory [17], are intentionally kept brief – the readers are referred to [16], [18].

1) *Offshore Wind Controls*: The individual wind turbines are based on doubly-fed induction generator (DFIG) and are represented by an aggregated model [16]. A simplified representation of the rotor side converter (RSC) controller with the inner current control loops is shown in Fig. 1(b). The RSC controls the real (P_W) and the reactive power (Q_W) output of the WF. The control input P_{Wmod}^* and Q_{Wmod}^* can be employed for supplementary PSS control.

2) *Offshore VSC Controls*: The Offshore VSC operates under $V_{ac} - f$ control, which transfers the wind power into the DC cable. Further operational constraints were imposed in the control loops: (i) a feed-forward term to change the frequency in case of over-voltage in the DC cable, signaling the wind turbines to reduce its power output and (ii) in case of an offshore fault, the current cannot be limited if the rectifier controlled only the voltage magnitude. A cascaded control in the voltage control loop is considered, Fig. 1(c).

3) *Onshore VSC Controls*: The onshore VSC operates in $V_{dc} - Q$ mode, maintaining constant DC bus voltage, and unity power factor at the point of connection (POC), as shown in Fig. 1(d). A decoupled current control strategy in the $d - q$ reference frame and standard PI controllers were used. Q_{INVmod}^* can be used for supplementary modulation of Q_{inv}^* towards damping power oscillations.

III. WIND FARM AND VSC-HVDC-BASED PSS: CHOICES AND OPERATIONAL CONSTRAINTS

There are several options for designing PSS for offshore WF connected via VSC-HVDC link, as illustrated in Fig. 2. The

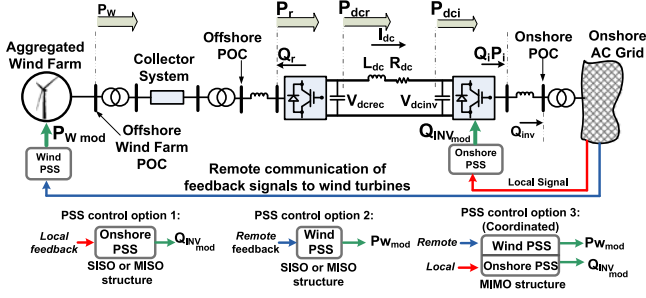


Fig. 2. Three PSS control options for a VSC-HVDC connected offshore WF is shown. Feedback signals using local (red) and remote (blue) are shown.

choice of control options and their practical implications are highlighted in the following subsections.

A. Control Option I: Onshore HVDC PSS (TSO Preferred)

The most convenient option for the onshore transmission system operator (TSO) is to modulate the reactive power ($Q_{INV\ mod}$) at the onshore VSC within their own jurisdiction - as depicted in Fig. 2. This prevents the need for supplementary control of offshore WF and thus, no dependence on the offshore transmission owner (OFTO). There is virtually no impact on the wind farm (i.e. no dynamic variation in active power output, turbine speed and DC link voltage) but the onshore reactive power and onshore bus AC voltage will experience larger dynamic variations. DC-link voltage modulation is possible, but not a desirable option in practice. Local measurements at the onshore converter station can be used as feedback signals if it has high modal observability [19]. Modulation of the reactive power reference of the onshore converter is henceforth referred to as *Onshore PSS*.

B. Control Option II: Offshore WF-Based PSS

An alternative option is to modulate the active power output of the offshore wind farm - henceforth referred to as *Wind PSS*. Since the offshore end is not synchronously connected to the onshore grid the inter-area oscillations are not observable there. Hence, the Wind PSS requires remote communication of the feedback signal from the onshore end and are therefore, vulnerable to problems (e.g. latency) in communication channels. For this reason, a time-delay model (a third-order Padé approximation) has to be included in the Wind PSS to represent the time delays associated with wide-area measurements. Modulation of WF real power $P_{W\ mod}$ as shown in Fig. 1(a) is the only suitable candidate for power oscillation damping. Neglecting converter losses and cable capacitance, and assuming perfect tracking:

$$V_{dcrec} = \frac{V_{dcinv}}{2} + \frac{1}{2} \sqrt{V_{dcinv}^2 + 4R_{dc}(P_W - P_{loss})} + \frac{L_{dc}}{2R_{dc}} \frac{d}{dt} \left\{ \sqrt{V_{dcinv}^2 + 4R_{dc}(P_W - P_{loss})} \right\} \quad (1)$$

Note that, the inverter control keeps the DC-link voltage V_{dcinv} constant. The assumptions in this derivation is that the dc voltage dynamics Cdv/dt in rectifier-end capacitor is neglected. Equation (1) shows that the larger the modulation in P_W , the

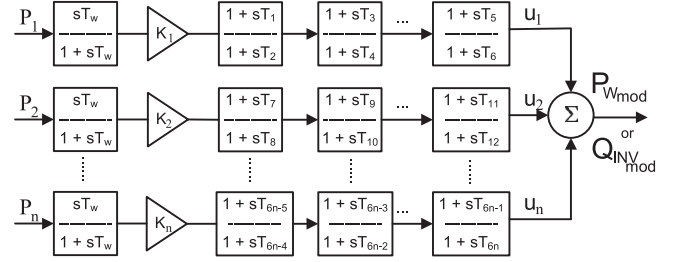


Fig. 3. General block diagram of n -input, 1-output controller (control options I, II).

higher the variation in the rectifier end DC-link voltage. From an operational standpoint, a large variation in the DC-link voltage is not desirable. The upper bound is limited due to the cable ratings and the lower bound by the saturation of modulation indices of the converter controls. The issues related to the rectifier DC-link voltage variation, converter rating, and allowable variation in turbine speed sets up the need for control coordination amongst the offshore wind farm and VSC-HVDC. A generic controller structure for PSS control options I, II is shown in Fig. 3.

C. Control Option III: Coordinated PSS

A coordinated design using both $P_{W\ mod}$ and $Q_{INV\ mod}$ as control inputs can be considered - henceforth referred to as *Coordinated PSS*. The following points are worth noting:

- 1) The overall damping duty will be distributed amongst the modulation of P_W^* and Q_{inv}^* .
- 2) For the same damping performance, the Coordinated PSS will use lesser variation of the onshore reactive power (Q_{inv}^*) and terminal AC voltage than the Onshore PSS (control option I), and likewise, reduced modulation in P_W^* compared to using Wind PSS (control option II).
- 3) DC-link voltage variation at the rectifier will be less due to smaller variation in P_W^* as seen from (1).

Similar to control option II, one loop of the Coordinated PSS requires remote communication of the feedback signal, as shown in Fig. 2. There are several options for designing a Coordinated PSS: i) centralized (full-structure) MIMO controller can be designed. However, controllers with such structures suffers due to the requirement of communicating the control signals from remote control centers to individual actuators, resulting in potential signal latencies and vulnerability to signal loss, or ii) decentralized (block-diagonalize) controller structure whereby the controllers are physically located at the actuator sites. Further advantages of decentralized over centralized include:

- 1) *Hardware simplicity*: The cost implications of a decentralized controller is much less than a centralized controller. A centralized controller for an $n \times n$ plant consists of $n!$ individual single-input-single-output (SISO) transfer functions.
- 2) *Tuning parameters*: decentralized controller architectures involve far less parameters, resulting in significant reduction in the time and cost of tuning.

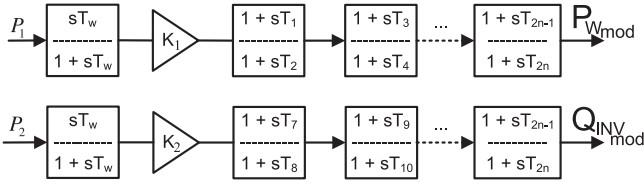


Fig. 4. General block diagram of n -input, n -output (decentralized) controller (control options III).

- 3) *Flexibility and tolerance to signal failure*: a decentralized structure allows the TSO to restructure the control system by bringing subsystems in and out of service individually as their decoupled, unlike a MIMO centralized controller which has cross-coupling terms. This could provide further robustness, as loss of one signal does not affect the remaining input-output control loops.

A generic controller structure for PSS control options III considering a MIMO controller decomposed into a set of decoupled SISO controllers, is shown in Fig. 4.

This paper proposes a robust homotopy approach that addresses the above issues.

IV. DESIGN OF ROBUST COORDINATED CONTROL USING HOMOTOPY

The control design is formulated in two-stages. In the first stage, a centralized controller, $G_C(s)$ is computed using methods reported in [13], [14]. In the second stage, the controller coefficient matrices are deformed from full-structure matrices defined by a centralized controller, to block-diagonal structure matrices which describes a decentralized control, $G_D(s)$.

A. Centralized (Full-Structure) Controller Design

Consider a linearized system model $G_i(s)$ expressed in state-space form as:

$$G_i(s) \triangleq \begin{bmatrix} A_i & B_i \\ C_i & 0 \end{bmatrix}; \quad A \in \mathfrak{R}^{n \times n}, B \in \mathfrak{R}^{n \times m}, C \in \mathfrak{R}^{m \times n} \quad (2)$$

where i represents the i^{th} operating condition. The objective is to synthesize a *full-structure* centralized linear output feedback controller $G_{C_i}(s)$ [13], where:

$$G_{C_i}(s) \triangleq \begin{bmatrix} A_{k_i} & B_{k_i} \\ C_{k_i} & 0 \end{bmatrix}; \quad A_k \in \mathfrak{R}^{n \times n}, B_k \in \mathfrak{R}^{n \times m}, C_k \in \mathfrak{R}^{m \times n} \quad (3)$$

The closed-loop system is represented by $\dot{\tilde{x}} = \tilde{A}_i \tilde{x}$, where, $\tilde{x} \in \mathfrak{R}^{2n}$ corresponds to the combined state vector of both the plant and the controller. The closed-loop transfer function is given by $T(s) = \tilde{C}_i(sI - \tilde{A}_i)^{-1} \tilde{B}_i$ with the system matrices $\tilde{A}_i, \tilde{B}_i, \tilde{C}_i$ given by:

$$\begin{bmatrix} \tilde{A}_i & \tilde{B}_i \\ \tilde{C}_i & \tilde{D}_i \end{bmatrix} = \begin{bmatrix} A_i & B_i C_{k_i} & B_i \\ B_{k_i} C_i & A_{k_i} & 0 \\ C_i & 0 & 0 \end{bmatrix} \quad (4)$$

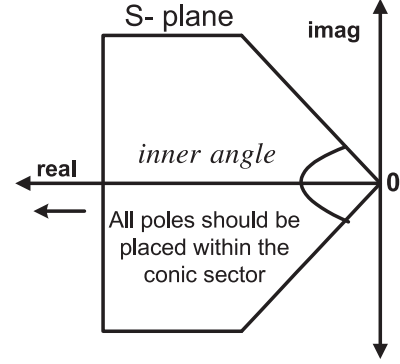


Fig. 5. Region for closed-loop poles with min. damping ratio, $\zeta = \cos\theta$.

To stabilize (2) by (3), is subject to finding $A_{k_i}, B_{k_i}, C_{k_i}$ and $\tilde{P}_i > 0$, to satisfy the Lyapunov:

$$\tilde{A}_i \tilde{P}_i + \tilde{P}_i \tilde{A}_i^T < 0 \quad (5)$$

The inequality in Equation (5) indicates that the matrix on the left hand side is a negative definite matrix. However, satisfying the inequality in (5), will only guarantee stability if the poles are located in the left half plane. This paper follows the practice established in [13] to reach a centralized (full-structure) controller in the Linear Matrix Inequalities (LMI) framework. This methodology satisfies several practical requirements with constraints included that guarantee the closed-loop system poles are placed within a conic-sector which ensures a minimum damping ratio $\zeta = \cos\theta$, shown in Fig. 5

The closed-loop system is guaranteed to have all its poles in the conic sector with apex at the origin and internal angle θ if and only if there exists a symmetric matrix $\tilde{P}_i > 0$ such that:

$$\begin{bmatrix} \sin\theta(\tilde{A}_i \tilde{P}_i + \tilde{P}_i \tilde{A}_i^T) & \cos\theta(\tilde{A}_i \tilde{P}_i - \tilde{P}_i \tilde{A}_i^T) \\ \cos\theta(\tilde{P}_i \tilde{A}_i^T - \tilde{A}_i \tilde{P}_i) & \sin\theta(\tilde{A}_i \tilde{P}_i + \tilde{P}_i \tilde{A}_i^T) \end{bmatrix} < 0 \quad (6)$$

The inequality in (6) contains the product $\tilde{A} \tilde{P}$ which are functions of the controller parameters A_k, B_k, C_k and the controller parameters themselves are function of \tilde{P} . This leads to $\tilde{A} \tilde{P}$ becoming non-linear in \tilde{P} . Following the practice outlined in [13], [20], it is possible to linearize the problem through change of controller variables. The resulting centralized controller is expressed as $G_{C_i}(s) = C_{ki}(sI - A_{ki})^{-1} B_{ki}$.

B. Decentralized (Block-Diagonal) Controller Design

In decentralized control, the design problems cannot be reduced to a feasibility problem for LMIs because of the structural constraint on the controller, i.e. *block-diagonal* forms of coefficient matrices. Hence, the concept of homotopy is applied to obtain a single *block-diagonal* controller starting from a single *full-structure controller* [15]. This paper proposes an extension to the standard homotopy approach, which allows a *single block-diagonal decentralized controller* to be reached from a *set of full-structure centralized controllers*, individually designed to ensure specified closed-loop performance under its respective operating condition.

Lets rewrite \tilde{A}_i from (5) as:

$$\tilde{A}_i \triangleq \underbrace{\begin{bmatrix} A_i & 0_{n \times \hat{n}} \\ 0_{\hat{n} \times n} & 0_{\hat{n} \times \hat{n}} \end{bmatrix}}_{\hat{A}_i} + \underbrace{\begin{bmatrix} 0_{n \times \hat{n}} & B_i \\ I_{\hat{n}} & 0_{\hat{n} \times p} \end{bmatrix}}_{\hat{B}_i} \underbrace{\begin{bmatrix} A_{ki} & B_{ki} \\ C_{ki} & 0_{p \times q} \end{bmatrix}}_{G_{C_i}} \underbrace{\begin{bmatrix} 0_{\hat{n} \times n} & I_{\hat{n}} \\ C_i & 0_{q \times \hat{n}} \end{bmatrix}}_{\hat{C}_i} \quad (7)$$

By substituting (7) into (5) this problem is equivalent to the existence of $\tilde{P} \in \mathbf{SR}^{n \times n}$ such that:

$$\tilde{P}_i > 0,$$

$$F(G_{C_i}, \tilde{P}_i) = (\hat{A}_i + \hat{B}_i G_{C_i} \hat{C}_i) \tilde{P}_i + \tilde{P}_i (\hat{A}_i + \hat{B}_i G_{C_i} \hat{C}_i)^T < 0 \quad (8)$$

F : a matrix variable expressed as a function of G_C and $\tilde{P} \in \mathbf{SR}^{n \times n}$: the set of symmetric $n \times n$ matrices.

Remark 1: A_k, B_k, C_k are *full-structure* matrices computed using LMIs as reported in [13]. However, since the objective here is to impose block-diagonal structure on these matrices, this leads to a problem with Bilinear Matrix Inequality (BMI).

Remark 2: The computational complexity for solving BMI problems is far greater than LMI problems since they are non-convex and can have multiple solutions.

It should be noted that the BMI in (8) can be treated as a double LMI. To solve this BMI problem, at each stage, groups of variables are fixed alternatively at the iterations to reduce the BMI to LMIs. In other words, the BMI constraints in (8) can be transformed into a set of LMI constraints by simply holding either G_C or \tilde{P} constant, such that only one variable needs to be solved at one time. Even if the original BMI is feasible, the induced LMIs could be unfeasible if G_D or \tilde{P} are set improperly. The transformation into LMIs can then be solved very efficiently [15] by adopting the idea of the homotopy method. Consider a real number λ which gradually varies from $0 \rightarrow 1$, and lets introduce a homotopy path to connect $H(G_{D_i}, \tilde{P}_i, \lambda_i)$ from *full-structure controller* (G_C) to *block-diagonal controller* (G_D) such that:

$$H(G_{D_i}, \tilde{P}_i, \lambda_i) = F\left((1 - \lambda_i) G_{C_i} + \lambda_i G_{D_i}, \tilde{P}_i\right) \quad (9)$$

where matrix variable H is a function of G_D, \tilde{P} and λ . Notice the term $(1 - \lambda)G_C + \lambda G_D$ in (9), with $\lambda = 0$, the result is a full-structure controller G_C (i.e. initial stage of the computation) and when $\lambda = 1$, it converges onto a decentralized structure G_D reflecting the desired final stage. Mathematically, that is equivalent to:

$$H(G_{D_i}, \tilde{P}_i, \lambda_i) = \begin{cases} F(G_{C_i}, \tilde{P}_i), \lambda = 0 \\ F(G_{D_i}, \tilde{P}_i), \lambda = 1 \end{cases} \quad (10)$$

The solution lies in the family of problems:

$$H(G_{D_i}, \tilde{P}_i, \lambda_i) < 0, \lambda_i \in [0, 1] \quad (11)$$

To carry out the homotopy method, find a solution to (G_D, \tilde{P}) at $\lambda = 0$. At this point, we set $\lambda = 0$ since G_D does not appear in (11) and setting $G_{D0} = 0$. If the increase in λ is kept sufficiently

Algorithm 1: *block-diagonalizing a full-structure controller.*

Input: A plant model $G(s)$, and a pre-designed centralized (full-structure) controller [13], $G_C(s)$.

Output: Decentralized (block-diagonal) controller, $G_D(s)$.

Parameters: Define M as the total number of homotopy steps. Set $M = 2$, an upper max $M_{max} = 2^{13}$.

Initialization: Set flag = 0, $\lambda_0 := 0$, $k := 0$ and $G_{D0} := 0$, and let \tilde{P}_0 be a solution of $H(G_{D0}, \tilde{P}_0, \lambda_0) < 0$.

while $k < M$ and $M \leq M_{max}$ **do**

$k := k + 1$;

$\lambda_k := k/M$;

if there exists solution G_D of

$H(G_D, \tilde{P}_{k-1}, \lambda_k) < 0$ **then**

 set $G_{Dk} := G_D$;

 solve for \tilde{P} under the constraint $H(G_{Dk}, \tilde{P}, \lambda_k) < 0$,

 set $\tilde{P}_k := \tilde{P}$;

 set flag := 1 and **break**;

end

if there exists solution of \tilde{P} of $H(G_{D_{k-1}}, \tilde{P}, \lambda_k) < 0$ **then**

 set $\tilde{P}_k := \tilde{P}$;

 solve for G_D under the constraint

$H(G_D, \tilde{P}_k, \lambda_k) < 0$, and set $G_{Dk} := G_D$;

 set flag := 1 and **break**;

end

 set $M := 2M$.

end

if $k = M$ or flag = 1 **then**

 The obtained pair (G_{Dk}, \tilde{P}_k) is the solution of the BMI (11). The desired decentralized controller is reached.

else

 The algorithm did **not** converge.

end

small (see λ_k in algorithm), the choice of G_{D0} will not affect the homotopy path in convergence.

The computational algorithm to arrive at a *block-diagonal* structure from a *full-structure controller* is outlined below.

Remark 3: The convergence rate of the algorithm to successfully reach a desired solution (G_D) depends on the choice of G_C which is not unique and defines the starting point of the homotopy path described by (9). The authors of [15] indicate random search in a parameterized set of \mathcal{H}_∞ controllers [21] is beneficial to find a suitable initial centralized \mathcal{H}_∞ controller for which the algorithm converges. Note that non-convergence of the algorithm for a specific G_C does not mean that a decentralized control problem has no solutions.

Remark 4: To improve the convergence of the algorithm, it is suggested to solve the two LMIs obtained by fixing one of the two variables in the BMI. It is not necessary to deal with the second one, but it is found to improve convergence.

Remark 5: As the solution to (11) is not unique, we could achieve the solution to the BMI (10) if go to the beginning the algorithm and start from $\lambda = 0$ and take an alternative homotopy path obtained with smaller number of homotopy steps M between $[0, 1]$.

Simultaneously designing for robustness: To capture realistic sets of control design specifications for power grids, we propose an extension to the above formulation to cater for robustness with changing operating condition. The operating condition of a power system changes frequently. Hence, linearizing the power

system for a number of (say, l) operating conditions allows for the design of controllers that provide robustness across a range of operating conditions. The algorithm proposed in the previous section transforms one single centralized controller designed based on a particular operating condition into one decentralized controller. A generalization for l operating conditions can be considered that results in a *single* decentralized controller obtained by considering $i = 1, 2 \dots l$ for equations (7)–(9).

To illustrate this, let us consider two centralized controllers G_{C1} and G_{C2} , designed based on power system models $(A_1, B_1, C_1, 0)$ and $(A_2, B_2, C_2, 0)$ respectively. Through two different homotopy paths $H(G_{D1}, \tilde{P}_1, \lambda_1)$ and $H(G_{D2}, \tilde{P}_2, \lambda_2)$, G_{D1} and G_{D2} are separately reached. By including a constraint of equating $G_{D1} = G_{D2}$, a single decentralized controller capable of stabilizing two operating conditions is obtained.

A generalization to ensure that a single decentralized controller, \mathcal{G}_D that stabilizes l operating conditions can be specified by defining the following system definitions for equations (8)–(9) and proceeding as before.

$$F(\mathcal{G}_C, \mathcal{P}) = (A + B\mathcal{G}_C C)\mathcal{P} + \mathcal{P}(A + B\mathcal{G}_C C)^T \quad (12)$$

$$H(\mathcal{G}_C, \mathcal{P}, \Lambda) = F((1 - \Lambda)\mathcal{G}_C + \Lambda\mathcal{G}_D, \mathcal{P}) \quad (13)$$

where,

$$\begin{bmatrix} A|B \\ C|0 \end{bmatrix} = \begin{bmatrix} \hat{A}_1 & 0 & \dots & 0 & \hat{B}_1 & 0 & \dots & 0 \\ 0 & \hat{A}_2 & \dots & 0 & 0 & \hat{B}_2 & \dots & 0 \\ \dots & \dots \\ 0 & 0 & \dots & \hat{A}_l & 0 & 0 & \dots & \hat{B}_l \\ \hline \hat{C}_1 & 0 & \dots & 0 & 0 & 0 & \dots & 0 \\ 0 & \hat{C}_2 & \dots & 0 & 0 & 0 & \dots & 0 \\ \dots & \dots \\ 0 & 0 & \dots & \hat{C}_l & 0 & 0 & \dots & 0 \end{bmatrix}$$

$$\hat{A}_i \in \mathbb{R}^{n_i \times n_i}, \hat{B}_i \in \mathbb{R}^{n_i \times 1}, \hat{C}_i \in \mathbb{R}^{1 \times n_i}, i = 1, 2, \dots, l$$

$$\mathcal{P} = \text{diag}(\tilde{P}_1, \tilde{P}_2, \dots, \tilde{P}_l); \Lambda = \text{diag}(\lambda_1, \lambda_2, \dots, \lambda_l)$$

$$\mathcal{G}_C = [G_{C1} G_{C2} \dots G_{Cl}]^T; \mathcal{G}_D = [G_{D1} G_{D2} \dots G_{Dl}]^T$$

The reason for selecting homotopy method over the usual iterative methods is that it has been observed that the domain of attraction of a solution point for iterative methods is usually much smaller than that for homotopy methods. However, due to the nature of the algorithm, non-convergence does not imply that a solution to the BMI problem does not exist. Model reduction can be applied to reduce the computational burden and hence improve the convergence time.

V. CASE STUDY I: 4-MACHINE, 2-AREA SYSTEM

For the first case study, the well-known 4-machine, 2-area test system is considered as the onshore network. The parameters used can be found [22].

An offshore WF is radially connected to bus 7 via a ± 150 kV bipolar VSC-HVDC link, as shown in Fig. 6. The WF comprises of 100 wind turbine generators (WTG) rated at 2 MW, 0.69 kV. An aggregated WTG model is used to represent the WF in this study. At full load, the wind farm transfers 200 MW through

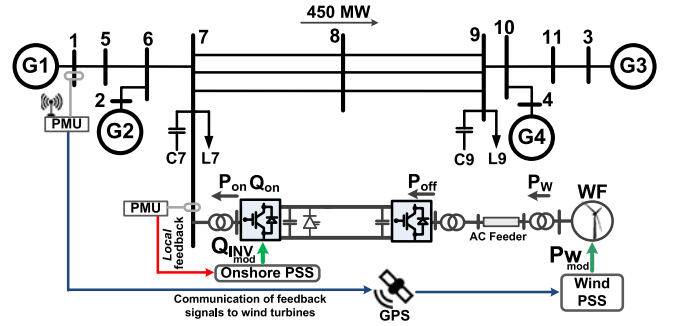


Fig. 6. 4-machine, 2-area test system with an offshore WF connected to bus 7 via VSC-HVDC link. Secondary control loops with PMU feedback signals.

a 33 kV AC feeder on to the DC side. A headroom provision (short-term overload) of 5% (10 MW) of the rated turbine power is specified. The duration over which the wind turbines are over-rated is of the order of several seconds [12].

A. Linearization of Models Through System Identification

Measurement-based system identification approaches such as numerical sub-space state-space system identification (N4SID) [23] can accurately estimate (identify) low-order linear state-space (A, B, C, D) models of power systems with several controllable devices (i.e. HVDC, wind farms). The linearized models can then be used for the design of controllers to improve the dynamic stability of the system. The methodology adopted here to obtain linearized state-space models are kept brief, as the formulation can be found in [24], [26].

A 25th-order linearized state-space model of the system including the WF and the DC-link was obtained using similar practice from [24], [26]. At full load (nominal wind speed), small-signal analysis revealed one lightly damped inter-area modes, $f = 0.61$ Hz, $\zeta = 2.2\%$ and two damped local modes with frequencies $f = 1.06$ Hz and $f = 1.09$ Hz. A wind turbine shaft-mode at $f = 1.68$ Hz with damping ratio $\zeta = 3.9\%$ is also observed.

B. Controllability and Observability Analysis

Observability measures were used to determine the most responsive input signals (stabilizing signals) from the 11 candidate bus signals to the inter-area mode [19]. All buses were considered as potential sites for PMU feedback, such that time-synchronized phase angle measurements data was available at the PSS site. The effectiveness of the WF and Onshore HVDC control inputs to the inter-area mode is determined from the Controllability measures, as shown in Fig. 8.

For this uni-modal system, local feedback signal at bus 7 was selected for the onshore VSC (although it has a lower observability measures than remote (i.e. bus 1) but this obviates the need for communication. The Wind PSS however requires communicating a remote feedback signal, and bus 1 was selected on the basis of the highest observability, as depicted in Fig. 6. For the set-up considered here, the “relative” controllability of the onshore VSC was found to be nearly twice as effective as the WF. These measures will vary with actuator location, the

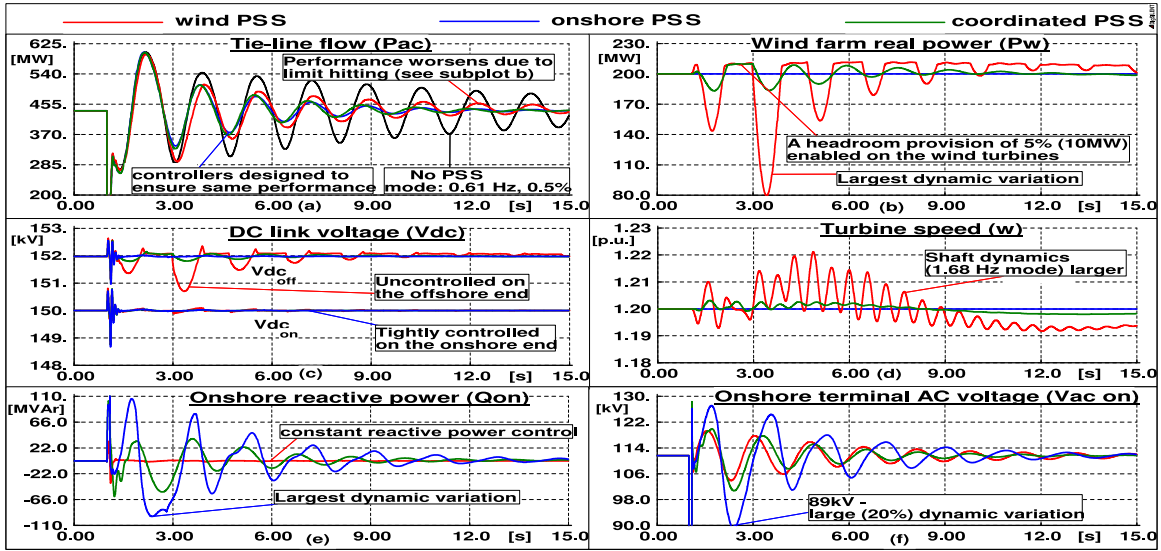


Fig. 7. Dynamic behavior of the system in response to a self-clearing 3-phase fault for 5-cycles on bus #9 without power oscillation damping control (black trace) and with i) Onshore PSS (blue traces), ii) Wind PSS (red traces), iii) Coordinated PSS (green traces). Plotted variables are denoted above each subplot.

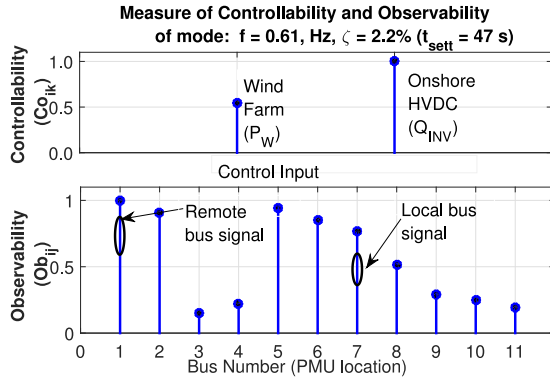


Fig. 8. Controllability and Observability indices (normalized) for the single inter-area mode. The observability indices indicate the phase angle of bus voltages measured at all 11 buses.

system mode, etc, and are important considerations prior to control design [19].

C. PSS Design

The following sub-sections outline the PSS design for the: a) onshore VSC, b) offshore wind-farm, and c) coordination between the offshore wind-farm and the onshore VSC. The controller objectives are to stabilize the lightly damped inter-area mode. All three control designs were intended to stabilize the inter-area mode within 12 s, as shown in Table I.

1) *SISO Controller Designs (Options I, II)*: The Wind PSS and Onshore PSS, can be designed using the regional pole-placement method introduced in Section IV-A (i.e. the first-stage to result in a centralized SISO controller). In all cases, the plant model used was reduced to 13th order model using balanced truncation technique. [23], [27]. Both controllers were further reduced to an 8th order while preserving the accuracy in the frequency range of interest. The PSS controller parameters for the Wind PSS is shown in Fig. 9.

TABLE I
SETTLING TIMES AND FREQUENCY OF THE SYSTEM INTER-AREA MODE WITH THE THREE CONTROL LOOPS

Onshore PSS		WF PSS		Coordinated PSS		Mode
t , sec	f , Hz	t , sec	f , Hz	t , sec	f , Hz	Type
10.6	0.605	10.1	0.611	9.7	0.612	Inter-area
8.5	1.064	8.5	1.064	8.5	1.064	Local
8.2	1.097	8.2	1.097	8.1	1.095	Local

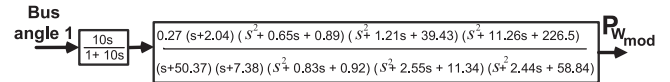


Fig. 9. Parameters of the Wind PSS (active power modulation using remote voltage phase angles of bus 1 as feedback signal).

2) *MIMO Controller Design (Option III)*: As the Coordinated PSS has two control-loops, the two-stage design proposed in Section IV was used here. In the first-stage, a coordinated, yet centralized controller is designed simultaneously for both the wind-farm and the onshore VSC station resulting in a *full-structure (centralized)* MIMO control of 13th order. In the second design-stage, the proposed Homotopy method is applied to *block-diagonalize* (decentralize) the full-structure controller, which essentially translates into two decentralized controllers, physically located at their respective actuator sites, as shown in Fig. 6. The final controller is of 8th order after further reduction using balanced truncation technique. The synthesized controller is a $2 \times$ SISO decentralized, yet coordinated controller, whereby each input-output channel is of 4th order, as shown in Fig. 10.

The \mathcal{H}_∞ disturbance attenuation level achieved in the case with centralized controller is 1.417, while the disturbance attenuation level achieved by the decentralized controller is 1.446. We find that homotopy algorithm converges when $M = 64$, when using the LMI toolbox of MATLAB.

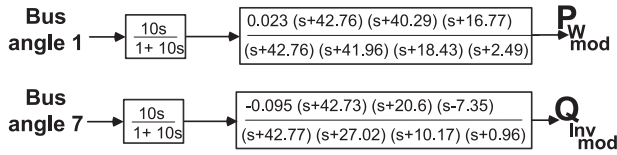


Fig. 10. Parameters of the Coordinated PSS (active power modulation of wind farm and reactive power of onshore VSC converter using phase angles of voltage at buses 1 and 7 as feedback signal).

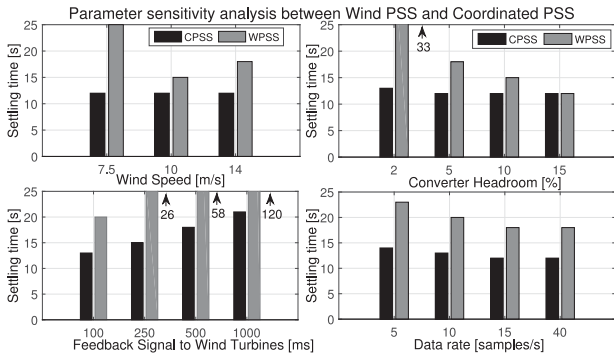


Fig. 11. Impact of different i) wind speeds, ii) WF converter headrooms, iii) latencies in signal communication to wind turbine actuators, iv) channel data-rates on the inter-area mode settling time considering CPSS and WPSS.

The closed-loop system with the decentralized controller was reasonably similar to that of the centralized controller.

D. Simulation Results

Dynamic simulation were conducted in DlgSILENT Power Factory to compare the system performance with the three PSS options, as illustrated in Fig. 7. A three-phase self-clearing fault at bus 9 for 5-cycles was considered as the disturbance.

Without PSS, the system response, as observed from the tie-line flow in Fig. 7(a) is highly oscillatory (black trace), whilst with either of the three PSSs, the oscillation settles within 12s. Although the system responses is seen to be similar, the variations in the WF power output and DC-link voltage are different. For instance, the real power output of the wind farm, shown in Fig 7(b), varies less with Coordinated PSS than wind PSS. In fact, with Wind PSS, the output power of the wind farm is often clipped at 210 MW (which corresponds to 5% headroom on the rated power of 200 MW), resulting in inferior system damping – red trace in Fig 7(a). From the results, the following observations can be made:

- 1) *Onshore PSS*: results in unacceptable onshore voltage variation and large dynamic variation on the onshore reactive power.
- 2) *Wind PSS*: results in repeated limit hitting, relatively large and rapid variation in turbine speed (which impacts the life of the turbine), and also offshore DC voltage. Modulation of WF real power is seen to interact with the torsional dynamics (shaft-mode) of wind turbines [28].
- 3) *Coordinated PSS*: is a compromise of the above two where the extent of dynamic variation of all the above variables is less than Wind PSS and Onshore PSS as the overall

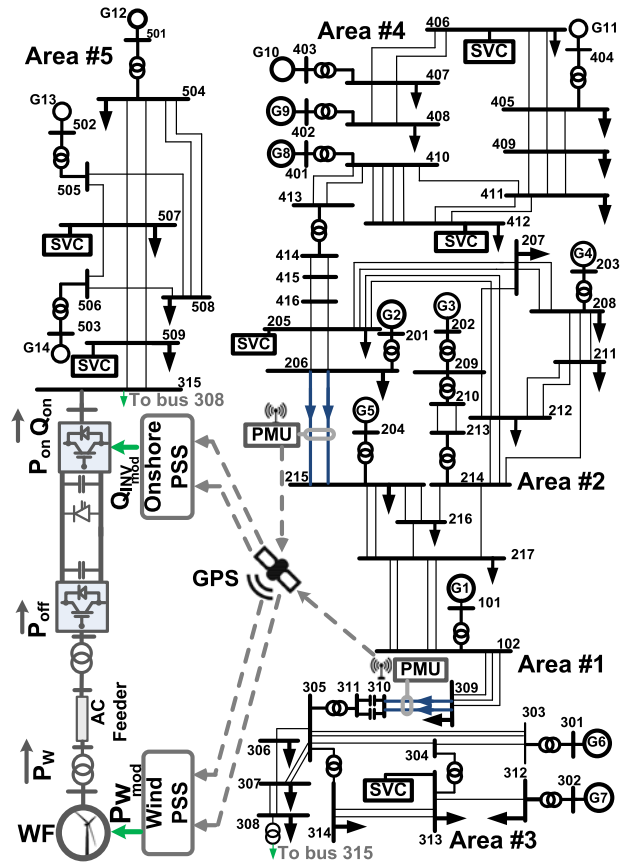


Fig. 12. 14-machine, 5-area test system with an offshore WF connected to bus 315 via a VSC-HVDC link. PSS controllers with PMU signals are shown.

TABLE II
SETTLING TIMES AND FREQUENCIES OF THE INTER-AREA AND LOCAL MODES OF THE 14-MACHINE, 5-AREA SYSTEM WITHOUT (WIND/ ONSHORE VSC) PSS CONTROL

Mode Type	Open-loop		Mode #	
	t, sec	f, Hz		
Inter-area	32.1	0.31	1	
	15.0	0.36	2	
	62.3	0.54	3	
	5.5	1.12	1	
	5.1	1.19	2	
	4.1	1.22	3	
	4.5	1.23	4	
	4.1	1.24	5	
	Local	5.6	1.29	6
		4.1	1.31	7
6.4		1.32	8	
5.7		1.40	9	
	4.2	1.54	10	

control duty is now shared between the wind farm and the onshore converter.

E. Parametric Sensitivity Analysis

Sensitivity analysis was conducted to determine the influence of changing system conditions or parameters on the settling times when deploying Wind PSS and Coordinated PSS.

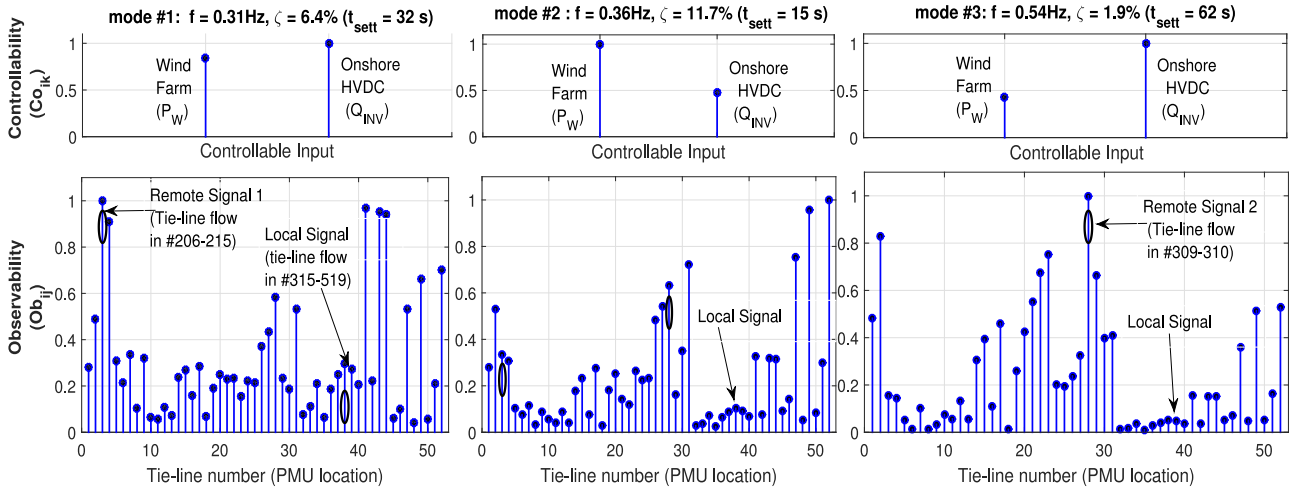


Fig. 13. Controllability and Observability indices (normalized) for each of the three inter-area modes. The upper subplots show how controllable a particular mode is from the actuator control inputs (i.e. Wind Farm and Onshore HVDC). The lower subplots indicate the level of observability a specific mode has at each of the 52 corresponding tie-lines.

The results are summarized, as shown in Fig. 11 for i) different wind speeds, ii) WF converter headrooms (over-rating), iii) latency in transmitting the signals to the individual wind turbines and iv) data rates.

It is found that Coordinated PSS is relatively robust to varying system conditions and parameters; whilst the performance deteriorates with Wind PSS. The condition where the feedback signal takes 1000 ms to get reflected at the individual wind turbines, the settling time with Coordinated PSS degrades to around 20 s, as seen in Fig. 11(c).

VI. CASE STUDY II: 14-MACHINE, 5-AREA SYSTEM

The proposed methodology was validated on a more complex network, representing the South-East Australian Power System, as shown in Fig. 12.

This system has been adopted as an IEEE benchmark system for small-signal analysis and the design of PSSs. The network parameters including the dynamics (excitation system, PSS, etc) can be found in [29]. The benchmark system is reinforced with an offshore WF connected through a DC-link to bus 315, as shown in Fig. 12. The WF consists of 225 DFIGs, aggregated to supply 450 MW at nominal wind speed. The converter ratings are chosen to match offshore supply.

A. Linearization of Models Through System Identification

A set of operating conditions were considered based on topological changes (e.g. outage of transmission lines). Outage of only one critical transmission line at a time was performed and the system subsequently linearized. Thus, a set of linear state-space models are obtained following similar practice used for the previous test case. In this paper, we considered i) nominal case, ii) planned outage of circuit 312 – 313 (critical circuit with very high flows).

Under the nominal case, small-signal analysis revealed two lightly damped inter-area modes, $f = 0.31$ Hz, $\zeta = 6.4\%$ and $f = 0.54$ Hz, $\zeta = 1.9\%$. A third inter-area mode with

$f = 0.36$ Hz mode also exists, but is reasonably damped at $\zeta = 11.7\%$. There also exists 10 local modes which are stabilized through the generator PSSs, as shown in Table II. A wind turbine shaft-mode at $f = 1.74$ Hz with damping ratio $\zeta = 3.6\%$ is also observed. Participation factor analysis show that 0.54 Hz mode was the result of machines in area #2 oscillating against those in area #3, whilst the 0.31 Hz mode results from machines in area #4 oscillating against those in areas #2 and #3.

B. Controllability and Observability Analysis

Two excitation inputs, P_W and Q_{INV} , and power flows across all 52 tie-lines were considered as candidate output signals. In other words, the open-loop system model has 2 inputs – 52 outputs. The results of the controllability/observability analysis, shown in Fig. 13, was used to assess the most appropriate input signals (stabilizing signal) for the WF and onshore VSC to achieve effective damping for all three inter-area modes. On this basis, tie-line flows in 206–215 and 309–310 were chosen as appropriate feedback signals (selected for all PSS designs), as shown the lower subplots. Interestingly, modes #1, #3 are more controllable from the Onshore VSC; whilst mode #2 is more controllable from the WF, as seen from the upper subplots. Unlike the test system in Fig. 6 where the local signal had sufficient modal observability for the Onshore PSS; in this network with 5 geographic areas, it can be seen in the lower subplots in Fig. 13 that the local signal yielded insufficient modal observability, and, if chosen, would require significantly larger converter overloading (headroom) than remote signals to achieve similar damping performance. Thus using remote signal(s) was the only viable option. The drawbacks of using remote feedback signals is later demonstrated under potential risks (e.g. latency, loss) in remote communication of those signals. The effectiveness of the PSS to damp power oscillations depends on several factors (e.g. system topology, load type and distribution, location of the WF and HVDC with the AC grids point of connection).

TABLE III
SETTLING TIMES AND FREQUENCY OF THE SYSTEM INTER-AREA MODES WITH THE THREE CONTROL LOOPS

Onshore PSS		WF PSS		Coordinated PSS		Inter-area
t , sec	f , Hz	t , sec	f , Hz	t , sec	f , Hz	Mode #
14.6	0.31	15.0	0.30	14.9	0.31	1
14.7	0.36	14.6	0.36	15.0	0.36	2
14.9	0.54	11.9	0.54	13.1	0.54	3

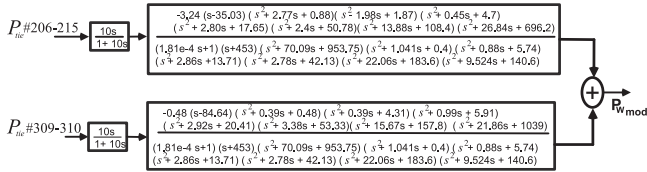


Fig. 14. Parameters of the Wind PSS (MISO centralized controller).

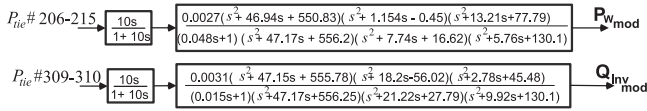


Fig. 15. Parameters of the Coordinated PSS (MIMO decentralized controller).

C. PSS Design

The following sub-sections outline the PSS design for the: a) onshore VSC, b) offshore wind-farm, and c) coordination between the offshore wind-farm and the onshore VSC. These three control options, as described in Section III were exercised separately to ensure all oscillatory modes settle by 15s, as shown in Table III.

1) *Multi-Input-Single-Output (MISO) Controller Designs (Options I, II)*: The Wind PSS and Onshore PSS, are designed using similar design approach as Case study I using the regional pole-placement method introduced in Section IV-A. The difference here is that the controller structure are fed with multiple input signals to cater for the multi-modes.

The synthesized controllers (Wind PSS and Onshore PSS) are both 30th order – similar to the system plant model. The final resulting controllers, after applying further reduction are 16th order multiple-input-single-output (MISO) centralized controllers. The PSS controller parameters for the Wind PSS is shown in Fig. 14.

2) *Multi-Input-Multi-Output (MIMO) Controller Design (Options III)*: The Coordinated PSS was designed using the method proposed in Section IV. First, a MIMO centralized controller – similar in size to the plant model of 30th order – is synthesized resulting in a 2-input 2-output full-structure controller. The model is then reduced to 14th order. The controller is then decomposed into two *locally decentralized* controllers by applying the homotopy-based algorithm, each with two remote signals (with highest modal observability) as the control inputs. The structure of each PSS channel is shown in Fig. 15 with each PSS channel of 7th order.

It was found that the homotopy algorithm converges when $M = 256$. The closed-loop frequency response of the 30th order *centralized* vs. 14th order *decentralized* controllers yield similar

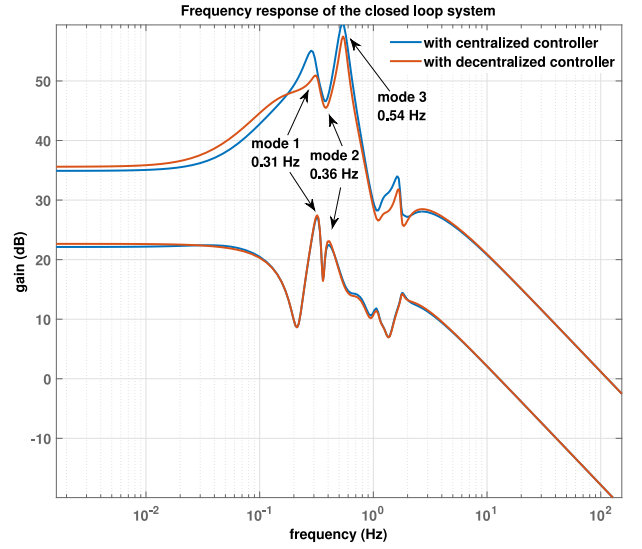


Fig. 16. Frequency response of the closed loop system with original centralized and reduced decentralized control.

performance (with expected performance deterioration due to block-diagonalizing the full-structure matrices), as shown in Fig. 16.

D. Simulation Results

To study the effectiveness of the three control options, a large set of credible fault disturbances were performed in DiGSILENT PowerFactory [17] on the test system shown in Fig. 12. One of the most severe disturbances stimulating poorly damped inter-area oscillations is a three-phase fault in one of the key transmission circuits. For temporary faults, the circuit breaker *auto-recloses* and normal operation is restored, otherwise, one or two lines might have to be taken out for maintenance.

To evaluate the performance of the designed controllers, simulations were carried out corresponding to fault scenarios *considered* in the design stage (Base case) and to verify its robustness, fault conditions *not considered* in the design, which include circuit outages (Case 1), and faults near the Onshore VSC station (Case 2) are simulated considering all three PSS control options. Finally, the dynamic behavior of the system with the three PSS control options is examined when potential risks in the communication systems in terms of latencies (Case 3) and complete signal loss (Case 4) occur in remote feedback signals.

A headroom provision of 10% of the rated turbine power is specified. The following disturbances were considered for all simulations with a three-phase solid fault for 100 ms (5 cycles) under the following scenarios:

- 1) *Base case*: Tie-line between buses 312-313 followed by auto-reclosing of the circuit breaker.
- 2) *Case 1*: bus 305 followed by outage of one of the tie-lines between buses 305-307.
- 3) *Case 2*: bus 315 followed by auto-reclosing of the circuit breaker (near Onshore VSC station).
- 4) *Case 3*: Impact of latencies in communicating remote signals to wind turbines and Onshore VSC station. Fault condition similar to ‘base case’.

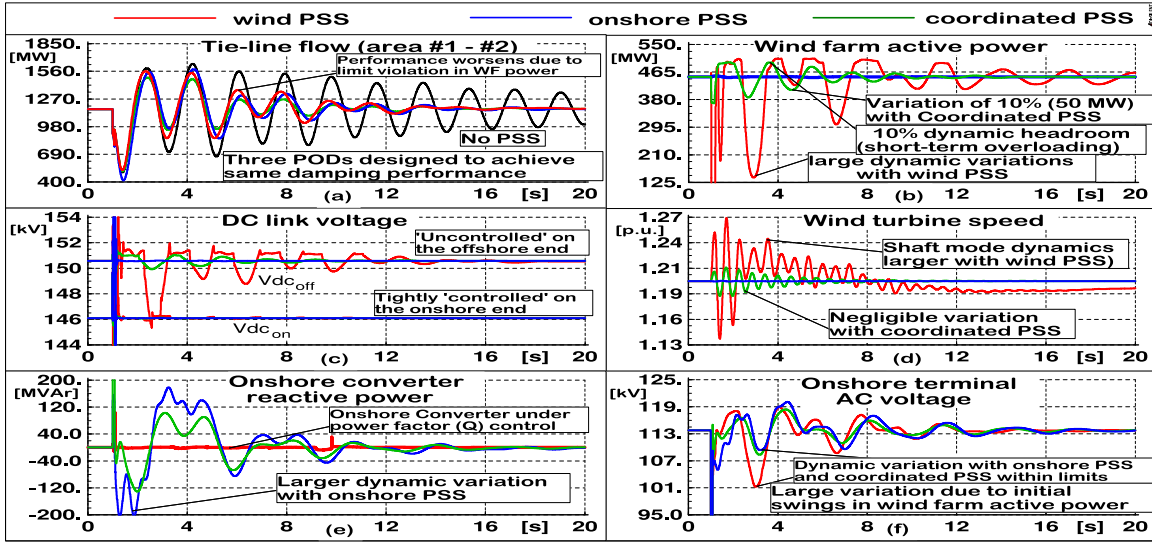


Fig. 17. Dynamic behavior of the system in response to 3-phase fault for 5-cycles on tie-line 312–313 followed by auto-reclosing of the circuit breaker. Without PSS control (black trace) and with i) Onshore PSS (blue traces), ii) Wind PSS (red traces) and iii) Coordinated PSS (green traces). Plotted variables are denoted above each subplot.

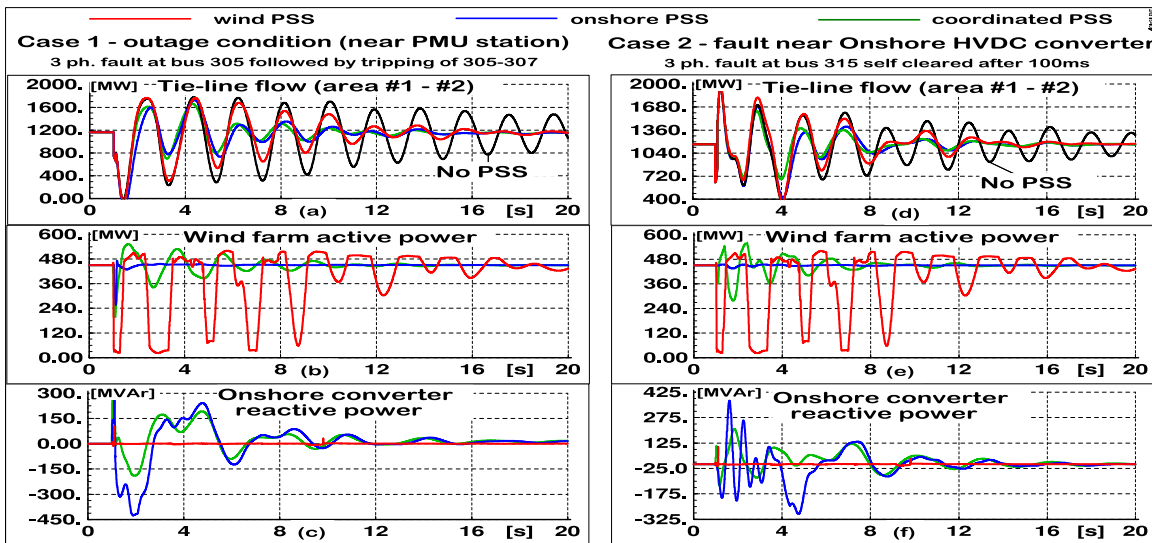


Fig. 18. Dynamic behavior of the system in response to a 3-phase fault on bus 305 for 5-cycles following by outage of one of the tie-lines between buses 305-307 (subplots a-c), and system response to a 3-phase fault at bus 315 followed by auto-reclosing of the circuit breaker (subplots d-f). Without PSS control (black trace) and with i) Onshore PSS (blue traces), ii) Wind PSS (red traces) and iii) Coordinated PSS (green traces).

5) *Case 4*: Impact of complete signal loss in communicating remote signals to the wind turbines and/or Onshore VSC station. Fault condition similar to ‘base case’.

The designed controllers are aimed to settle the multiple inter-area oscillations within 15 s (performance criteria) following the disturbances. Moreover, it should be able to achieve this following any of the above disturbances (robustness) although the design is based on a base case operating condition (no outage). The disturbances under all cases were created 1 s after the start of the simulation. The follow section highlights remarks regarding the findings:

1) *Base Case*: The dynamic response of the system following the disturbance is shown in Fig. 17. As in the previous case study, all three PSS control options are able to damp the multiple inter-area modes within 15 s. Similar to the previous case study,

larger dynamic variation in reactive power of the onshore VSC is required with Onshore PSS than Coordinated PSS. However, the resulting variation in onshore AC voltage is similar due to low Q-V sensitivity at the onshore bus.

2) *Case 1 (Robustness)*: It can be seen from Fig. 18(a) that inter-area oscillations settle within the desired time frame of 15 s for the post-fault operating condition not considered in the controllers designs and thus satisfy the robustness requirement. This is a severe outage condition as the circuit carries high power transfer. Wind PSS requires around 20 s to damp the inter-area modes which is due to repeatedly hitting the dynamic overloading limits, as seen in Fig. 18(b). Larger dynamic variation (swings) in reactive power of the onshore VSC is required with Onshore PSS (+240/–420 MVar) than Coordinated PSS (± 190 MVar), as seen in Fig. 18(c).

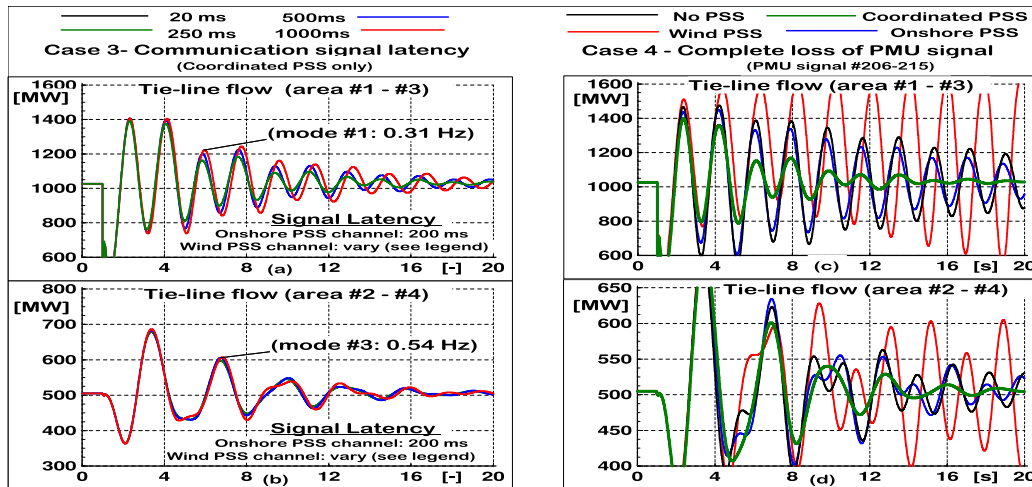


Fig. 19. Impact of latencies in communicating remote signals to wind turbines and Onshore VSC station are shown in subplots (a)-(b). Subplot (c)-(d) shows impact on the system after loss of signal 206-215 to all three PSS controllers. A 3-phase fault for 5-cycles on tie-line 312-313 followed by auto-reclosing of the circuit breaker. Description of traces denoted above the plots.

3) *Case 2 (Robustness)*: A fault at bus 315 which is near the Onshore VSC is simulated. The results shown in Fig. 18(d)–(f) substantiate the conclusions drawn in case 1.

4) *Case 3 (Signal Latency)*: In the previous case study shown in Section V, only the locally available signals were considered for feedback control due to good observability of the inter-area mode. In the present case study, the benefits of using remote signals (in favor of local) available from the phasor measurement units (PMUs) were justified in Section VI-B. However, this comes at a cost of potential adverse impact when problems (e.g. signal latency, complete loss of PMU signal) occur in remote communication system. For the nominal case, a standard PMU delay of 20 ms (corresponding to 50 Hz sampling) is considered for both channels of the Coordinated PSS.

To study the effect of signal latency, we considered for this study a fixed delay of 200 ms for the Onshore PSS, whilst varying the latency to the Wind PSS from 250 ms to 1000 ms. As shown earlier, participation factor analysis revealed which groups of generators contributed to the lightly damped inter-area modes (0.31 and 0.54 Hz). The 0.31 Hz mode manifests itself in the tie-line flows between areas #1 – #3, whilst the 0.54 Hz mode in the flows between areas #2 – #4.

Figs. 19(a), (b) illustrates the impact of signal latencies up to a delay of 1000 ms on the two critical inter-area modes. The damping slightly deteriorates considering delays up to 1000 ms for the Wind PSS channel. Of course, in the rare event that the delay to the Onshore PSS channel (which in this case study has a prominent role in damping the modes) exceeds beyond 200 ms, then the closed-loop response would deteriorate noticeably. In such cases delays need to be considered explicitly in the design stage although this aspect was not considered in this paper.

5) *Case 4 (Signal Loss)*: Another important aspect is the effectiveness of the controllers in the event of a signal communication failure. The problem that is addressed here is what is the impact on the closed-loop system when adopting a (i) centralized controller (i.e. Onshore PSS and Wind PSS) against that of (ii) a decentralized controller (i.e. Coordinated PSS) when a signal loss occurs, as depicted in Fig. 20.

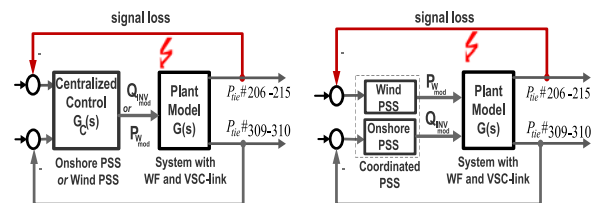


Fig. 20. Closed-loop system with i) centralized controller structures (left), (b) decentralized control structure (right). Feedback signal loss shown in red.

Fig. 19(c)&(d) illustrates the impact of loss of a feedback signal (206 – 215) on the settling times of the two lightly damped inter-area modes (0.31 and 0.54 Hz) under all three control options. Under Wind PSS (red traces) the closed-loop performance is far worse with respect to its open-loop case (black traces) as the mode has shifted very close to the imaginary axis. This is due to the cross-coupling between the control loops through the off-diagonal terms of the controller. With Onshore PSS (blue traces) similar effect can be seen, but the damping performance shifts towards the open-loop case. However, with the decentralized case, the ability to damp the modes are retained. This is because the control structure is block-diagonal and individual control loops are *decoupled* from each other, which is not only easier to implement in a decentralized architecture, but also ensures a certain level of performance through the healthy control loops in the event of loss of one or more (but not all) remote feedback signals. The results from this section substantiate the conclusions drawn from the previous test network; albeit on a more practical system with several inter-area modes.

VII. CONCLUSION

The effectiveness of coordinated power oscillation damping control through offshore wind farms and onshore VSC-HVDC converters that connect those wind farms, was presented. To that end, an algorithm using the idea of homotopy method was used which deforms the controller from a centralized controller to a decentralized (block-diagonal) controller. Similar damping performance could be achieved with damping contribution from

only the onshore VSC or the offshore wind farm. However, it has been shown using two case studies that the coordinated control is advantageous in terms of reducing AC side the voltage excursions at the onshore converter station while respecting the over-loading capacity of the HVDC and wind turbine converters.

REFERENCES

- [1] "Network code for HVDC connections and DC-connected power park modules," European Network of Transmission System Operators, 2014. [Online]. Available: <https://www.entsoe.eu/major-projects/network-code-development/high-voltage-direct-current/Pages/default.aspx>
- [2] J. L. Domínguez-García, O. Gomis-Bellmunt, F. D. Bianchi, and A. Sumper, "Power oscillation damping supported by wind power: A review," *Renew. Sustain. Energy Rev.*, vol. 16, no. 7, pp. 4994–5006, 2012.
- [3] F. M. Hughes, O. Anaya-Lara, N. Jenkins, and G. Strbac, "Control of DFIG-based wind generation for power network support," *IEEE Trans. Power Syst.*, vol. 20, no. 4, pp. 1958–1966, Nov. 2005.
- [4] J. Domínguez-García, F. Bianchi, and O. Gomis-Bellmunt, "Analysis of the damping contribution of power system stabilizers driving wind power plants," *Wind Energy*, vol. 17, no. 2, pp. 267–278, 2014.
- [5] M. Zhixin, F. Lingling, D. Osborn, and S. Yuvarajan, "Control of DFIG-based wind generation to improve interarea oscillation damping," *IEEE Trans. Energy Convers.*, vol. 24, no. 2, pp. 415–422, Jun. 2009.
- [6] A. E. Leon and J. A. Solsona, "Power oscillation damping improvement by adding multiple wind farms to wide-area coordinating controls," *IEEE Trans. Power Syst.*, vol. 29, no. 3, pp. 1356–1364, May 2014.
- [7] M. Singh, A. J. Allen, E. Muljadi, V. Gevorgian, Y. Zhang, and S. Santoso, "Interarea oscillation damping controls for wind power plants," *IEEE Trans. Sustain. Energy*, vol. 6, no. 3, pp. 967–975, Jul. 2015.
- [8] Y. Liu, J. R. Gracia, T. J. King, and Y. Liu, "Frequency regulation and oscillation damping contributions of variable-speed wind generators in the U.S. Eastern Interconnection (EI)," *IEEE Trans. Sustain. Energy*, vol. 6, no. 3, pp. 951–958, Jul. 2015.
- [9] M. Mokhtari and F. Aminifar, "Toward wide-area oscillation control through doubly-fed induction generator wind farms," *IEEE Trans. Power Syst.*, vol. 29, no. 6, pp. 2985–2992, Nov. 2014.
- [10] Y. Wang, J. Meng, X. Zhang, and L. Xu, "Control of PMSG-based wind turbines for system inertial response and power oscillation damping," *IEEE Trans. Sustain. Energy*, vol. 6, no. 2, pp. 565–574, Apr. 2015.
- [11] L. Zeni *et al.*, "Power oscillation damping from VSC-HVDC connected offshore wind power plants," *IEEE Trans. Power Del.*, vol. 31, no. 2, pp. 829–838, Apr. 2016.
- [12] G. Tarnowski, P. C. Kjaer, R. Laerke, F. Iov, R. Teodorescu, and A. Adamczyk, "Power plant and energy storage system for provision of grid ancillary services," WIPO Patent PCT/DK2013/050 032, Feb. 7, 2013.
- [13] R. Ramos, L. Alberto, and N. Bretas, "A new methodology for the coordinated design of robust decentralized power system damping controllers," *IEEE Trans. Power Syst.*, vol. 19, no. 1, pp. 444–454, Feb. 2004.
- [14] B. Chaudhuri and B. Pal, "Robust damping of multiple swing modes employing global stabilizing signals with a TCSC," *IEEE Trans. Power Syst.*, vol. 19, no. 1, pp. 499–506, Feb. 2004.
- [15] G. Zhai, M. Ikeda, and Y. Fujisaki, "Decentralized H_∞ controller design: A matrix inequality approach using a homotopy method," *Automatica*, vol. 37, no. 4, pp. 565–572, 2001.
- [16] M. A. Poller, "Doubly-fed induction machine models for stability assessment of wind farms," in *Proc. IEEE Power Tech Conf.*, Bologna, Italy, 2003, vol. 3, 6 pp., doi: 10.1109/PTC.2003.1304462.
- [17] "Digsilent powerfactory 15.2," 2015. [Online]. Available: <http://www.digsilent.de>
- [18] Ö. Göksu, J. N. Sakamuri, C. A. Rapp, P. Sørensen, and K. Sharifabadi, *Cluster Control of Offshore Wind Power Plants Connected to a Common HVDC Station*, *Energy Procedia*, vol. 94, Sep. 2016, pp. 232–240, ISSN 1876-6102, [Online]. Available: <http://dx.doi.org/10.1016/j.egypro.2016.09.230>
- [19] I. Kamwa, R. Grondin, and Y. Hebert, "Wide-area measurement based stabilizing control of large power systems—a decentralized/hierarchical approach," *IEEE Trans. Power Syst.*, vol. 16, no. 1, pp. 136–153, Feb. 2001.
- [20] M. Chilali and P. Gahinet, " H_∞ design with pole placement constraints: An LMI approach," *IEEE Trans. Autom. Control*, vol. 41, no. 3, pp. 358–367, Mar. 1996.
- [21] J. C. Doyle, K. Glover, P. P. Khargonekar, and B. A. Francis, "State-space solutions to standard H_2 and H_∞ control problems," *IEEE Trans. Autom. Control*, vol. 34, no. 8, pp. 831–847, Aug. 1989.
- [22] P. Kundur, *Power System Stability and Control* (The EPRI Power System Engineering Series). New York, NY, USA: McGraw-Hill, 1994.
- [23] I. Kamwa, G. Trudel, and L. Gerin-Lajoie, "Low-order black-box models for control system design in large power systems," *IEEE Trans. Power Syst.*, vol. 11, no. 1, pp. 303–311, Feb. 1996.
- [24] N. Zhou, J. W. Pierre, and J. F. Hauer, "Initial results in power system identification from injected probing signals using a subspace method," *IEEE Trans. Power Syst.*, vol. 21, no. 3, pp. 1296–1302, Aug. 2006.
- [25] J. F. Hauer *et al.*, "Use of the WECC WAMS in wide-area probing tests for validation of system performance and modeling," *IEEE Trans. Power Syst.*, vol. 24, no. 1, pp. 250–257, Feb. 2009.
- [26] Y. Pipelzadeh, B. Chaudhuri, and T. C. Green, "Role of Western HVDC link in stability of future Great Britain (GB) transmission system," in *Proc. 2015 IEEE Power & Energy Soc. General Meeting*, Jul. 2015, pp. 1–5.
- [27] C. A. Beattie and S. Gugercin, "A trust region method for optimal H[2] model reduction," in *Proc. 2009 48th IEEE Conf. Decision Control Held Jointly With 2009 28th Chin. Control Conf.*, Dec. 2009, pp. 5370–5375.
- [28] L. Fan, H. Yin, and Z. Miao, "On active/reactive power modulation of DFIG-based wind generation for interarea oscillation damping," *IEEE Trans. Energy Convers.*, vol. 26, no. 2, pp. 513–521, Jun. 2011.
- [29] M. Gibbard and D. Vowles, *Simplified 14-Generator Model of the South East Australian Power System*. Adelaide, Australia: Univ. Adelaide, 2014, pp. 1–138.



Yousef Pipelzadeh (S'09–M'12) received the Ph.D. degree in power systems from Imperial College London, London, U.K., in 2012. He is a Research Associate in Imperial College London, and the Business Development Manager of Manitoba HVDC Research Center, U.K. He is recognized by the British Standard Institute as a U.K. Principle Expert, and is an active member of the European Commission (Cenelec working group TC8X/WG 06) developing the guidelines and standards on HVDC Grids. He has particular interests in power system dynamics and offshore DC networks. He is an active member of IET and CIGRE.



Nilanjan Ray Chaudhuri (S'06–M'08–SM'16) received the Ph.D. degree in power systems from Imperial College London, London, U.K., in 2011. He is a Member of the IEEE Power and Energy Society. He holds five US patents and two European Patents with numerous pending applications. He is the lead author of the book *Multi-Terminal Direct Current Grids: Modeling, Analysis, and Control* (Wiley/IEEE Press, 2014), and an Associate Editor of the IEEE TRANSACTIONS ON POWER DELIVERY. He received the National Science Foundation CAREER Award in

2016.



Balarko Chaudhuri (M'06–SM'11) received the Ph.D. degree in electrical and electronic engineering from Imperial College London, London, U.K., in 2005, where he is currently a Senior Lecturer at the Control and Power Research Group. His research interests include power systems stability, grid integration of renewables, HVDC, FACTS, demand response, and smart grids. He is an Editor of the IEEE TRANSACTIONS ON SMART GRID and an Associate Editor of the IEEE SYSTEMS JOURNAL and *Elsevier Control Engineering Practice*. He is a Fellow of the

Institution of Engineering and Technology and a Member of the International Council on Large Electric Systems.



Tim C. Green (M'89–SM'02) received the B.Sc.(first class Hons.) degree in engineering from Imperial College London, London, U.K., in 1986 and the Ph.D. degree from the Heriot-Watt University, Edinburgh, U.K., in 1990. He is a Professor of Electrical Power Engineering in Imperial College London and the Director of the Energy Futures Lab. His research interest is in formulating the future form the electricity network to support low-carbon futures. A particular theme is how the flexibility of power electronics and control can be used to accommodate new generation patterns and new forms of load, such as EV charging, as part of the emerging smart grid. He has particular interests in offshore DC networks and of management of low voltage networks.